RSC Advances

PAPER

View Article Online
View Journal | View Issue

Cite this: *RSC Adv.*, 2016, **6**, 12348

Imidazolines containing single-, twin- and triple-tailed hydrophobes and hydrophilic pendants $(CH_2CH_2NH)_nH$ as inhibitors of mild steel corrosion in CO_2–0.5 M NaCl†

Mohammad A. J. Mazumder,*[a] Mazen K. Nazal,[a] Mohamed Faiz[b] and Shaikh A. Ali[a]

Received 13th October 2015
Accepted 22nd January 2016

DOI: 10.1039/c5ra21276f

www.rsc.org/advances

Inhibition of mild steel corrosion in CO_2–0.5 M NaCl (40 °C, 1 atm; 120 °C, 10 bar) by a new series of imidazolines having single-, twin- and triple-tailed phenyl substituents at C(2) and N(1) pendants of $CH_2CH_2NH_2$ and $(CH_2CH_2NH)_2CH_2CH_2NH_2$ have been examined. Imidazolines containing twin-tailed (3,5-dioctyloxyphenyl) hydrophobes outperformed their single- and triple-tailed counterparts as well as two commercial imidazolines. The triamine pendant imparted better inhibition at higher temperature and pressure. The XPS study confirmed the presence of an imidazoline film covering the metal surface. The imidazolines prefer to be adsorbed on the metal surface rather than micellization.

1. Introduction

The oil and gas industries, at every stage of production involving extraction, refining, storage and transportation through pipelines, face severe corrosion problems, which must be alleviated by the application of corrosion inhibitors.[1] CO_2 corrosion, induced by its presence in the produced fluids, is one of the most prevalent forms of attack, which causes failures of carbon steels.[2] Significant progress has been made in pinpointing factors and conditions like temperature, pH, CO_2 pressure, *etc.*, which influence the complicated mechanism of CO_2 corrosion.[3,4] However, a story unraveling the inhibition mechanism and its kinetics, which would help design efficient chemical inhibitors to combat corrosion, still remains incomplete.[4–6]

In an oxygen-free anaerobic aqueous solution, CO_2 is in equilibria with H_2CO_3, HCO_3^- and H^+, as described by eqn (1) and (2):

$$CO_2\,(g) \rightleftharpoons CO_2\,(aq) \quad (1)$$

$$CO_2\,(aq) + H_2O \rightleftharpoons H_2CO_3\,(aq) \rightleftharpoons HCO_3^-\,(aq) + H^+\,(aq) \quad (2)$$

The corrosive reactions on the metal surface are the results of the following half-cell reactions at the cathodic sites:[7,8]

$$2H^+\,(aq) + 2e \rightleftharpoons H_2\,(g) \quad (3)$$

$$2H_2O + 2e \rightleftharpoons 2OH^-\,(aq) + H_2 \quad (4)$$

$$2H_2CO_3\,(aq) + 2e \rightleftharpoons 2HCO_3^-\,(aq) + H_2\,(g) \quad (5)$$

$$2HCO_3^-\,(aq) + 2e \rightleftharpoons 2CO_3^{2-}\,(aq) + H_2\,(g) \quad (6)$$

and iron dissolution at the anodic sites:

$$Fe\,(s) \rightleftharpoons Fe^{2+}\,(aq) + 2e \quad (7)$$

Combination of relevant ions then forms several iron(II) compounds as shown by eqn (8)–(11):[7,9,10]

$$Fe^{2+}\,(aq) + 2OH^-\,(aq) \rightleftharpoons Fe(OH)_2\,(s) \quad (8)$$

$$Fe(OH)_2\,(s) \rightleftharpoons FeO\,(s) + H_2O \quad (9)$$

$$Fe^{2+}\,(aq) + 2HCO_3^-\,(aq) \rightarrow Fe(HCO_3)_2\,(aq) \quad (10)$$

$$Fe(HCO_3)_2\,(aq) \rightleftharpoons FeCO_3\,(s) + H_2O\,(aq) + CO_2\,(g) \quad (11)$$

Dry CO_2 is not corrosive to mild steel pipelines,[11] it is the carbonic acid (H_2CO_3) which, at the same pH, is more corrosive than aqueous HCl.[12] The predominant cathodic reduction at pH < 4 is believed to be reaction (3), while at pH values in the range 5–6, reactions (5) or (6) takes place.[13] The pitting corrosion caused by CO_2 leads to the deposition of layers of hydroxides and carbonates on the metal surface. At higher temperatures, the rate of cell reactions (3), (5) and (6) decreases as a consequence of decreased solubility of CO_2 in the aqueous layer as represented by eqn (1), while the rates of reactions (4), (7) and (11) increase.[7] Advantageous passivation of steel surface by the film composed

[a]*Chemistry Department, King Fahd University of Petroleum and Minerals, Dhahran 31261, Saudi Arabia. E-mail: jafar@kfupm.edu.sa; Web: http://faculty.kfupm.edu.sa/CHEM/jafar/; Fax: +966-13-860-4277; Tel: +966-13-860-7836*

[b]*Physics Department, King Fahd University of Petroleum and Minerals, Dhahran 31261, Saudi Arabia*

† Electronic supplementary information (ESI) available. See DOI: 10.1039/c5ra21276f

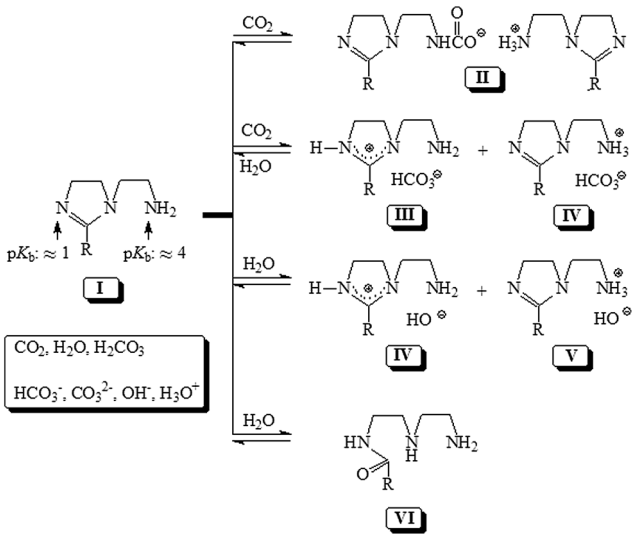

Scheme 1 IMs in an aqueous CO_2 system.

of the corrosion products such as water–insoluble $FeCO_3$ and $Fe(HCO_3)_2$ minimizes the corrosion rate of mild steel.[14]

Most corrosion inhibitors used in oilfields have motifs of surfactant molecules having a hydrophilic polar head and a hydrophobic tail. Adsorption of surfactants onto metal surface leads to the formation of a protective layer, which decreases the wettability of steel surface, while their accumulation at the oil–water decreases the oil–water interfacial tension thereby making it easier for the oil to entrain the water.[15] Imidazolines (IMs) **I**, containing sub-structures of a hydrophilic IM ring having electron-rich amidine (N=C–N) motifs embedded in it, a hydrophobic alkyl chain at C(2) and a hydrophilic pendant at N(1), are widely used as inhibitors in CO_2-satuarted saline media (Scheme 1).[16]

While the nitrogens in amidine motifs are weakly nucleophilic, they are strong bases akin to organic bases like 1,8-diazabicyclo[5.4.0]undec-7-ene (DBU) (pK_b 1.1) and 1,5-diazabicyclo[4.3.0]non-5-ene (DBN) (pK_b 0.5),[17] all having the same amidine motifs. The pendant NH_2 is a weaker base ($pK_b \approx 4$) but a stronger nucleophile enabling it to form carbamate salt

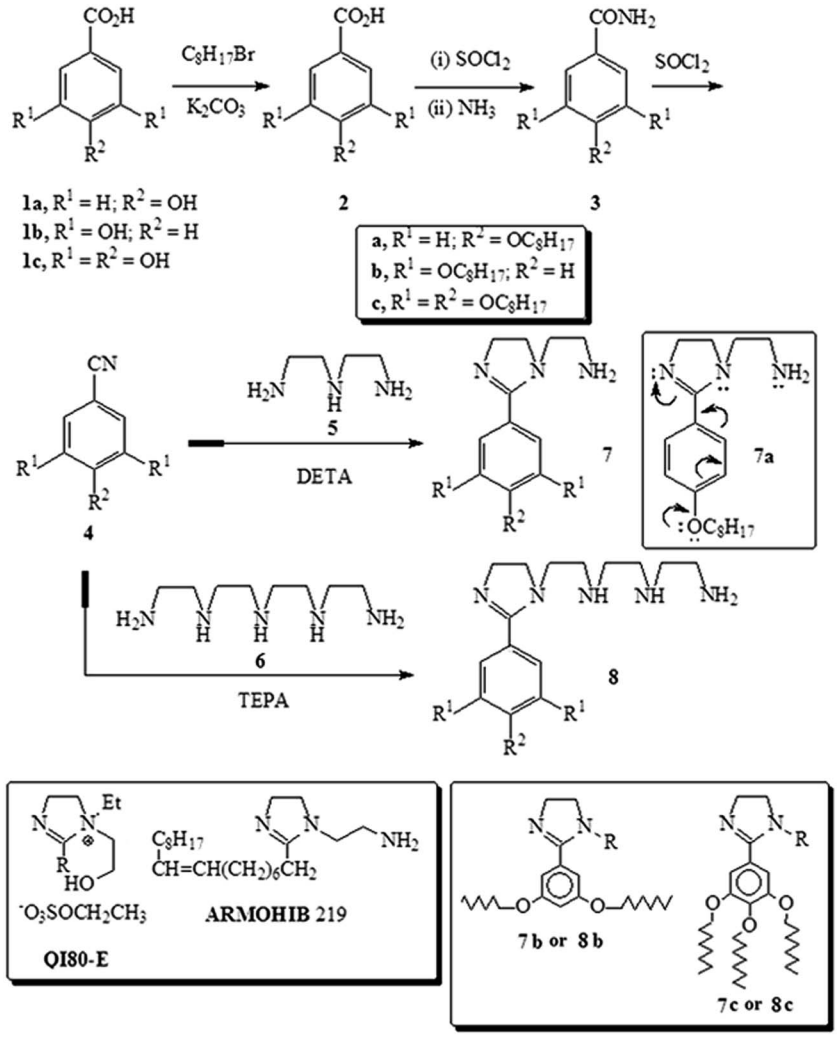

Scheme 2 Synthesis of IMs.

II in the presence of CO_2.[18–20] As a base, all the nitrogens can abstract a proton from carbonic acid (*i.e.* aqueous CO_2, H_2CO_3) to form protonated **III** and **IV**.[20–22] Amidine motifs in IMs on partial hydrolysis is converted into amides **V**.[21] The IM–CO_2 (aq) system thus contains several compounds (**I–V**), H_2CO_3, CO_2, H_2O and ionic species such as HCO_3^-, CO_3^{2-}, OH^-, and H_3O^+. It is indeed an arduous task to unlock the poorly understood mechanism of corrosion inhibition in such a complex scenario where the system consists of a complex maze of neutral and ionic species let alone the effects of the presence of Cl^- ions, temperature, partial pressure of CO_2, corrosion products among many other factors.

There are contradictory reports on the relative importance of each sub-structure in IMs in corrosion inhibitions.[23,24] Bis-IM and IM compounds have been shown to form a compact inhibitor layer to reduce the cathodic controlled CO_2 corrosion.[25,26] The protonated form of a thioureido IM acts as an inhibitor of CO_2 corrosion by its adsorption on the negatively charged steel surface thereby shifting the potential of zero charge (PZC) to positive direction.[27] Corrosion inhibition performance of several 2-undecyl-2-IMs has indicated that the hydrophilic *N*-pendants have remarkable influence on the inhibition efficiency.[28] A study of corrosion inhibition of an amido-IM on mild steel in CO_2–saturated NaCl solution has revealed that its inhibition efficiency was enhanced by addition of iodide ions due to synergistic effect.[29] The presence of double bonds in the hydrocarbon chains at C(2) and functional groups in *N*-pendants[30] as well as polycentric adsorption sites has been shown to increase inhibition efficiency by the formation of a chemically adsorbed film on the surface of the metal.[31] For two IMs, both having a heptadecyl hydrophobe at C(2), the one having the longer *N*-pendant of $(CH_2CH_2NH)_3H$ performed better than the other having $CH_2CH_2NH_2$ pendant; they are shown to cover the steel surface prior to reaching their critical micelle concentrations (CMCs).[32] A novel series of IMs having hydrophobes of octyloxy, dodecyloxy- and octadecyloxyphenyl substituent at C(2) and *N*-pendants of $(CH_2CH_2NH)_nH$ has been shown to impart very good inhibition of CO_2 corrosion of mild steel in CO_2–0.5 M NaCl.[20] For '*n*' values of 1 and 3, there was no change in inhibition efficiencies, while increasing hydrophobe chain lengths imparted increasing corrosion inhibition.

In the current work, it is our objective to synthesize a series of IMs having C(2) single-, twin- and triple-tailed phenyl substituents and *N*-pendants of $(CH_2CH_2NH)_nH$ (n = 1 and 3) (Scheme 2). The presence of electron-donating octyloxy tail(s) would increase the electron density in the amidine motifs and thus retard its hydrolysis to amides by making the amidine C less susceptible to nucleophilic attack. The study, assisted by potentiodynamic polarizations, electrochemical impedance spectroscopy (EIS), gravimetric weight loss, surface tension and X-ray photoelectron spectroscopy (XPS), would permit us to examine the effects of the hydrophobic tails and length of *N*-pendants on the inhibition in CO_2–0.5 M NaCl solutions. We anticipate an interesting outcome to enrich the current knowledge of the inhibition process.

2. Experimental

2.1. Materials

p-Hydroxybenzoic acid, α-resorcyclic acid, gallic acid, 1-bromooctane, cysteine hydrochloride, silica gel 100 and thionyl chloride from Fluka Chemie AG, and diethylenetetramine (DETA) (99.5%) from Aldrich chemical were used as received. Tetraethylenepentamine (TEPA) (~60% purity) from Aldrich chemical was purified as before,[32] and IMs **7a** and **8a** were synthesized using literature procedures.[20] 3,5-Dioctyloxy- and 3,4,5-trioctyloxy-benzoic acid **2b** and **2c** were prepared as described.[33]

2.2. Physical methods

Melting points are recorded in an Electrothermal Apparatus. IR spectra were recorded on a Perkin Elmer 16F PC FTIR spectrometer. NMR spectra were taken in $CDCl_3$ (+TMS) on a JEOL LA 500 MHz NMR spectrometer. Elemental compositions were determined with an Elemental Analyzer (Carlo-Erba: model 1106).

2.3. Synthesis

2.3.1. General procedure for the synthesis of di-, and tri-octyloxybenzamides (3b, 3c). The detailed procedure for the synthesis of octyloxybenzamides **3b** and **3c** given in the ESI.†

2.3.2. General procedure for the synthesis of di-, and tri-octyloxybenzonitriles (4b, 4c). The detailed procedure for the synthesis of di-, and tri-octyloxybenzonitriles **4b** and **4c** given in the ESI.†

2.3.3. General procedure for the synthesis of 1-(2-aminoethyl)-2-(di-, tri-alkoxyphenyl)-2-imidazolines (7b, 7c). A solution of di- or tri-octyloxybenzonitriles (**4b** or **4c**) (25 mmol) and DETA **5** (62 mmol) containing cysteine-HCl (100 mg) in a RB flask fitted with an U-tube containing mineral oil was stirred under N_2 at 145 °C for 1 h. After adding another portion of cysteine-HCl (100 mg), the mixture was heated at 145 °C for an additional 1 h. After the ceasing of the evolution of NH_3 gas, the cooled reaction mixture in CH_2Cl_2 (50 mL) was carefully washed with water (3 × 300 mL). After drying the organic layer and removal of the solvent, IM (**7b** or **7c**) was obtained as a pinkish liquid/semisolid. The detailed characterization of **7b** and **7c** is given in ESI.†

2.3.4. General procedure for the synthesis of IMs 8b, 8c. The reaction described under Section 2.3.3 was repeated under same conditions using TEPA **6** (62 mmol) instead of DETA **5** keeping all other materials unchanged. Similar work up afforded **8b** or **8c** as a pinkish liquid/semisolid. The detailed characterization of **8b** and **8c** is provided in the ESI.†

2.4. Specimens

Corrosion tests by electrochemical measurements in CO_2–0.5 M NaCl solution were performed using working electrode prepared from mild steel having the composition (in wt%): 0.089% (C), 0.34% (Mn), 0.037% (Cr), 0.022% (Ni), 0.007% (Mo), 0.005% (Cu), 0.005% (V), 0.010% (P), 99.47% (Fe). Mild

steel sheet of 1 mm thickness was machined to a flag shape having a 3 cm stem, which was insulated by Araldite paint (affixing material). The remaining exposed area of 2 cm^2 was abraded with emery papers (100, 400, 600 and 1500 grit size), washed with acetone, deionized water and finally acetone. Prior to their use, an ultrasonic bath was used to treat the specimens for 5 min followed by washing with distilled water.

Mild steel coupons A and B measuring $\approx 2.5 \times 2.0 \times 0.1$ cm^3 for the autoclave tests, have the following elemental analyses (in wt%):

2.4.1. Coupon A. 0.082% (C), 0.016% (Cr), 0.207% (Mn), 0.062% (Ni), 0.029% (Cu), 0.012% (Mo), 0.032% (Si), 0.011% (Co), 0.045% (Al), <99.3% (Fe).

2.4.2. Coupon B. 0.168% (C), 0.038% (Cr), 0.495% (Mn), 0.034% (Ni), 0.074% (Cu), 0.237% (Si), 0.014% (P), 0.024% (S), 0.011% (Co), 0.080% (Al), <98.6% (Fe).

Mild steel, also known as carbon steel, is the steel in which the main interstitial alloying constituent is carbon. Low-carbon steel, containing approximately 0.05–0.25% carbon, is now the most common form of steel for many applications because its price is relatively low while it provides acceptable material properties. We have used three kinds of mild steel: coupons for electrochemical measurements and coupons A and B for the autoclave tests having carbon content of 0.089%, 0.082% and 0.168%, respectively, to cover a range of carbon content.

2.5. Solutions

Test solutions of CO_2–0.5 M NaCl for the inhibition study in the presence and absence of IMs at 40 °C (1 atm) as well as at a higher pressure (10 bar) and temperature (120 °C) were deaerated by purging with 99.999% N_2 (20 min) followed by continuously bubbling with 99.999% pure CO_2 (20 min) to avoid corrosion caused by oxygen. During polarization measurements, the gentle flow of CO_2 was maintained above the surface of the solution without agitating the bulk of the solution. The addition of $NaHCO_3$ (100 mg L^{-1}) in the test solutions maintain their pH between 5.0 and 5.5 to avoid any change in the corrosion mechanism.

2.6. Electrochemical measurements

2.6.1. Tafel extrapolations. The experiments were performed in a 750 mL round-bottom flask fitted with a mild steel working electrode, saturated calomel electrode (SCE), and a counter electrode of graphite ($\approx$5 mm diameter). The test solutions of 0.5 M NaCl (250 mL) were saturated with CO_2 (1 atm, 40 °C). After connecting all three electrode cells to the potentiostat, the polarization curves were recorded by a computer controlled potentiostat–galvanostat (Auto Lab, Booster 10A-BST707A, Eco Chemie, Netherlands) where the cutoff current was set at 10 mA. A computer (Windows 7) loaded with NOVA (Version 1.8) software processed the data. The working electrode was pre-corroded for 30–60 min to achieve a stable open circuit potential, after which, a scan of $\pm$250 mV with respect to the open circuit potential E_{corr} is conducted at a rate of 0.5 mV s^{-1}.

2.6.2. Linear polarization resistance (LPR) method. The LPR measurements were carried out using the same cell described above to obtain polarization resistance values from current potential plots by scanning through a potential range of $\pm$10 mV around E_{corr}.

2.6.3. Electrochemical impedance spectroscopy (EIS). The impedance measurements were carried out in a 750 mL round-bottom flask fitted with a three electrodes system as described under Section 2.6.1. A solution of 0.5 M NaCl (250 mL) containing 100 mg L^{-1} $NaHCO_3$ were saturated with CO_2 (1 atm) at 40 °C was used as a test solution. The impedance plots were recorded using a computer controlled potentiostat-galvanostat (Auto Lab, Booster 10A-BST707A, Eco Chemie, Netherlands). The impedance measurements were carried out at the open circuit potential with a frequency scan ranging from 100 kHz to 50 mHz and amplitude value of 10 mV. The impedance curves were fitted and the electrochemical equivalent circuit obtained by NOVA (Version 1.8) software.

2.7. Autoclave experiments

The weight-loss measurements were performed by immersing carbon-steel coupons in a 0.5 M NaCl solution (250 mL) at 120 °C in the presence of CO_2 (10 bar) was conducted in a R&D Autoclave Bolted Closure System (Autoclave Engineers, model # 401C-0679) for 48 h. The detailed experimental procedure with or without inhibitors (200 ppm) is described in our earlier work.[34]

2.8. Measurement of surface tension

The surface tension of the IM samples in CO_2–0.5 M NaCl solution at 40 °C were measured by a PHYWE surface tensiometer (Germany) as described.[20]

2.9. The standard free energy of micelle formation (ΔG°_{mic})

The ΔG°_{mic} of the IM surfactant is given by eqn (12),[35]

$$\Delta G^{\circ}_{mic} = RT \ln(C_{cmc}) \quad (12)$$

where R, T and C_{cmc} represent the gas constant, temperature and surfactant concentration in mol L^{-1} at the critical micelle concentration (CMC).

2.10. X-ray photoelectron spectroscopy

The metal coupons of dimension of $2.5 \times 2.0 \times 0.1$ cm^3 having the same composition to those used in the electrochemical tests were cleaned (*vide supra*) and then immersed in a CO_2–0.5 M NaCl–IM (100 ppm) at 40 °C for 6 h. The coupons were then dried under N_2 after carefully rinsing with distilled deionized water. The XPS analysis was carried out as described[20] using a Thermos Scientific X-ray photoelectron spectrometer (model # Escalab 250 Xi). The C 1s peak at 285.4 eV was selected to be the reference peak. Deconvoluted XPS spectra were obtained using a non-linear least squares algorithm.

3. Results

3.1. The IMs' synthesis

As outlined in Scheme 2, mono-, di- and tri-hydroxybenzoic acids **1** was alkylated with octyl bromide to give the corresponding octyloxybenzoic acids **2**, which were converted into nitriles **4** *via* benzamide **3** in excellent yields. Heating a mixture of nitrile **4** with DETA **5** or TEPA **6** in the presence of catalyst cysteine. HCl at 145 °C led to the formation of the IMs **7** and **8**, respectively, in excellent yields. The IMs were readily identified by ^{1}H and ^{13}C NMR spectroscopy. The ^{1}H and ^{13}C NMR spectra of some of the representative IMs **7c**, **8a** and **8c** are displayed in Fig. 1 and 2, respectively. The characteristic Hs marked a–c are readily identifiable in the proton spectra. Aromatic Hs appeared at expected places with anticipated multiplicities. The carbon spectra revealed the presence of four signals for the carbons of **7c** marked as a–d, while for the TEPA-derived IMs **8a** and **8c**, all eight carbons marked a–h appeared as non-overlapping signals in the spectra. Thus a series of IMs having single-, twin- and triple-tailed octyloxyphenyl groups and different *N*-substituents has been synthesized to study the effects of C(2) substituents and N(1) pendants; their efficacies were compared with that of two commercial inhibitor samples: QI80-E (R = C_{12} to C_{22}) from Materials Performance and ARMOHIB 219 from AKZO NOBEL (Scheme 2).

3.2. Electrochemical measurements

3.2.1. OCP *vs.* time measurements. In this study, the effect of immersing time on the open circuit potential (OCP) *versus* saturated calomel electrode (SCE) in CO_2 saturated 0.5 M NaCl solution was explored for the mild steel coupon in the absence (blank) and presence of different concentrations (1 and 100 ppm) of **7b** and **8b** at 40 °C. The results obtained for the variation of OCP with time are depicted in Fig. 3. In the absence and presence of inhibitors, the OCP changes very quickly towards the less negative value and become stable after 20 min. Hence, the 30 minutes of mild steel immersion time was used in all subsequent electrochemical measurements.

3.2.2. Tafel extrapolation. The extrapolation data for the mild steel corrosion in a CO_2–0.5 M NaCl are summarized in Table 1. Some representative Tafel plots are shown in Fig. 4; usual analysis of each pair of Tafel plots provided the i_{corr} and

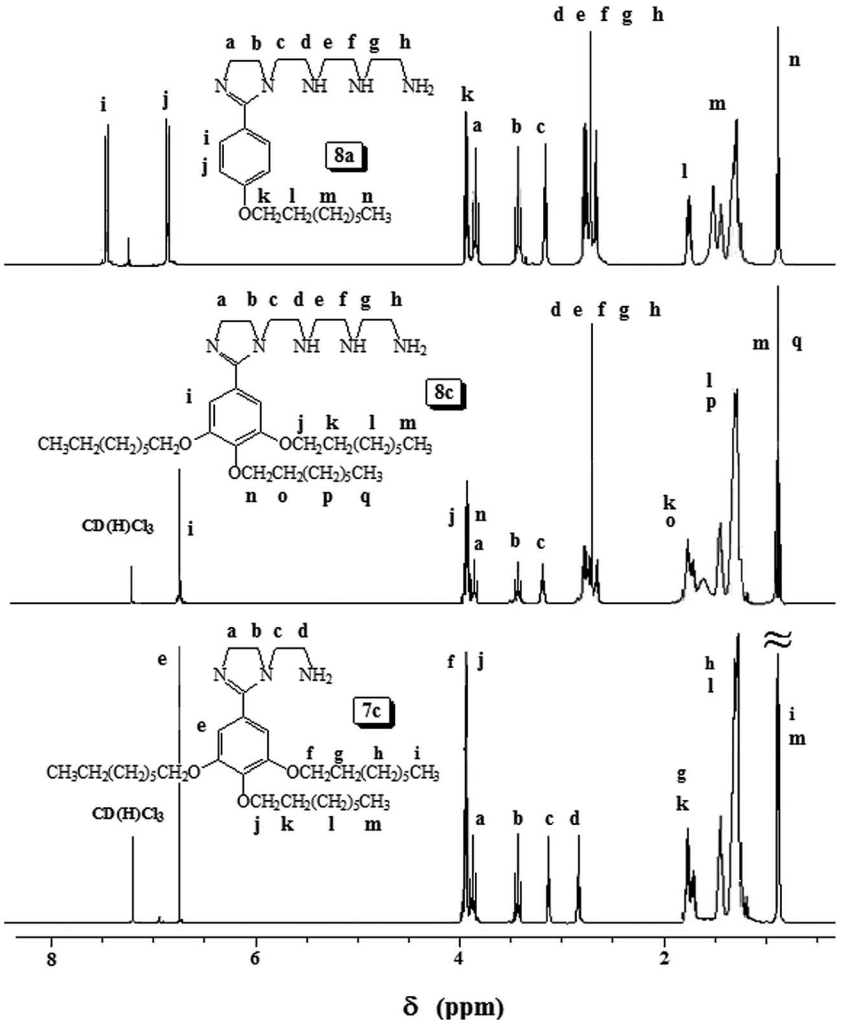

Fig. 1 ^{1}H NMR spectra of the IMs **7c**, **8a** and **8c** in $CDCl_3$.

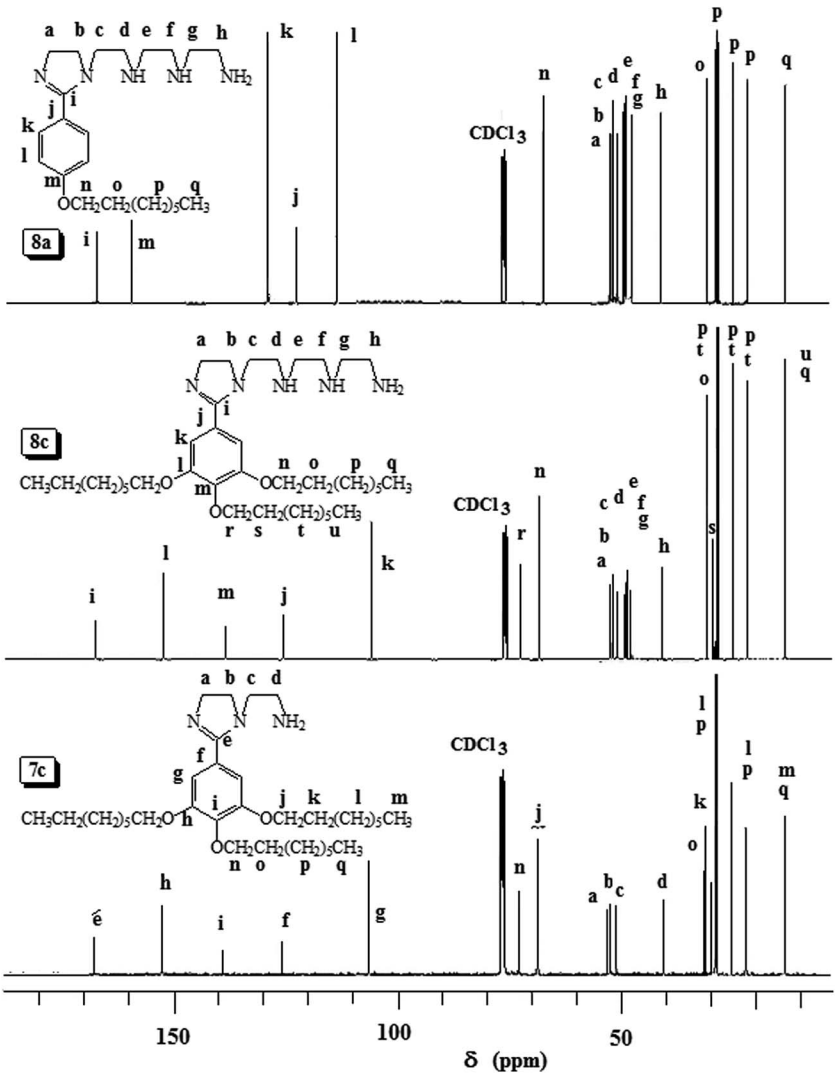

Fig. 2 ^{13}C NMR spectra of the IMs **7c**, **8a** and **8c** in the δ 40–55 ppm range in $CDCl_3$.

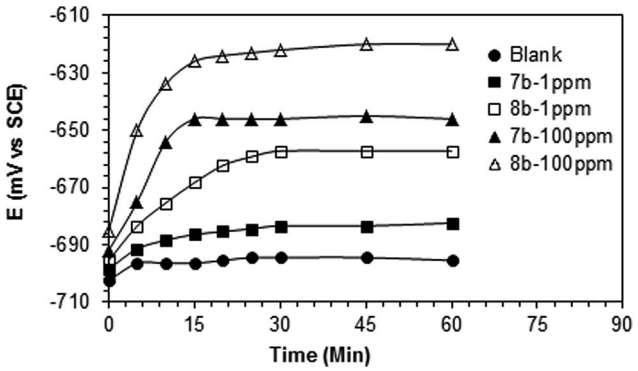

Fig. 3 Variation of OCP of mild steel with time of immersion in CO_2–saturated 0.5 M NaCl containing different concentrations (1 and 100 ppm) of **7b** and **8b** at 40 °C.

E_{corr} values. The cathodic Tafel lines were extrapolated with respect to free corrosion potential by using an automated linear curve fitting Nova (version 1.8) software.

3.2.3. LPR. The inhibition efficiency (η%) from LPR technique was calculated using eqn (13):

$$\eta(\%) = \left(\frac{R'_p - R_p}{R'_p}\right) \times 100 \quad (13)$$

where R_p and R'_p represent the polarization resistance values in inhibitor-free and inhibitor-added CO_2–0.5 M NaCl at 40 °C, respectively. The results are summarized in Table 1.

3.2.4. Impedance measurements. The Randles electrochemical equivalent circuit shown in Fig. 5 was used to represent the Nyquist diagrams of solution-mild steel interface in absence and presence of inhibitors (**7b**, **8b**). The fitted equivalent circuit included three elements; a solution resistance (R_s), polarization resistance (R_p) and constant phase element (CPE). The R_s resulted from the potential drop between the mild steel electrode and the reference electrode and its value obtained from crossing the semicircle with the real part (Z') axis at high frequency. The polarization resistance includes a charge transfer resistance and a diffusion layer resistance at the surface of the mild steel electrode.[36] The polarization resistance

Table 1 Results of Tafel plots and LPR of a mild steel sample in CO_2–0.5 M NaCl containing inhibitors **7(a–c)** and **8(a–c)** at 40 °C

	Concentration		Tafel plots					LPR[e]
Sample	ppm (by wt)	μM	E_{corr} *vs.* SCE (mV)	β_a (mV dec^{-1})	β_C (mV dec^{-1})	i_{corr} (μA cm^{-2})	η^a (%)	η^a (%)
Blank[b]	0	0	−700	41.2	−258	103.6	–	–
7a[c]	1	3.15	−694	75.2	−141	49.9	51.8	58.9
	5	15.7	−683	40.0	−166	38.5	62.8	63.7
	10	31.5	−677	44.3	−172	30.9	70.1	67.5
	20	63.0	−671	63.9	−181	24.6	76.2	73.6
	50	157	−667	45.6	−139	17.3	83.3	84.2
	100	315	−665	36.4	−123	8.32	92.0	90.8
7b[c]	1	2.24	−691	32.5	−165	49.5	52.2	61.0
	5	11.2	−678	53.7	−161	36.1	65.2	68.9
	10	22.4	−674	48.1	−149	26.7	74.2	74.1
	20	44.9	−667	52.1	−168	18.3	82.3	84.1
	50	112	−654	32.5	−171	9.30	91.0	92.1
	100	224	−643	55.4	−157	4.02	96.1	96.7
7c[c]	1	1.74	−693	66.5	−103	54.2	47.7	56.1
	5	8.71	−686	28.1	−167	45.3	56.3	62.3
	10	17.4	−680	46.6	−80.6	31.4	69.7	68.1
	20[d]	34.8	−673	42.3	−81.5	28.8	72.2	71.5
	50[d]	87.1	−661	64.9	−177	22.7	78.1	79.9
	100[d]	174	−655	64.0	−146	13.5	87.0	85.4
8a[c]	1	2.48	−671	61.1	−249	49.2	52.5	44.6
	5	12.4	−660	32.4	−146	41.2	60.3	58.1
	10	24.8	−648	57.5	−228	29.1	71.9	68.1
	20	49.6	−645	35.8	−183	22.5	78.2	74.7
	50	124	−641	69.2	−124	19.6	81.1	82.6
	100	248	−637	66.7	−238	9.2	91.1	90.2
8b[c]	1	1.88	−667	71.9	−156	48.5	53.2	48.9
	5	9.40	−658	46.9	−184	38.3	63.0	67.0
	10	18.8	−653	50.3	−176	26.2	74.7	76.3
	20	37.6	−642	46.6	−618	19.6	81.1	84.2
	50	94.0	−632	51.3	−169	11.4	89.0	93.8
	100	188	−627	52.6	−190	3.9	96.2	97.1
8c[c]	1	1.52	−697	65.8	−112	56.9	45.1	49.1
	5	7.58	−689	50.4	−133	47.3	54.3	56.2
	10	15.2	−675	58.3	−180	31.0	70.1	62.3
	20[d]	30.3	−664	65.9	−155	27.9	73.1	67.1
	50[d]	75.8	−659	21.3	−148	20.5	80.2	78.3
	100[d]	152	−650	45.3	−182	14.5	86.0	84.1

[a] Inhibition efficiency (*i.e.*, η) = surface coverage θ. [b] The blank was a CO_2–0.5 M NaCl solution. [c] Inhibitor sample was dissolve in 0.5 cm^3 2-propanol, and added with 249.5 cm^3 blank solution. [d] Cloudy solution. [e] Polarization resistance for blank: 89.7 Ω cm^2.

resulted at the mild steel electrode surface R'_p excluding the potential drop between the two electrodes can be calculated using eqn (14).

$$R'_p = R_p - R_s \quad (14)$$

The η% of the inhibitor can be determined from the corrosion resistance R_p in inhibitor-free solution and R'_p in inhibitor-added solution using eqn (13).

The double layer capacitance and coating capacitance modeled with a CPE that represents a non-ideal capacitance, which depends on a degree of surface homogeneity (n).[37] Due to inadequate homogeneity of the un-inhibited and inhibited mild steel surface, n value in eqn (15) is lower than 1 and the capacitance (c) is replaced with symbol Q.

$$Z = \frac{1}{(i\omega Q)^n} \quad (15)$$

where Z is the imaginary part, ω is the frequency (Radian) and i is the current (A).

Fig. 6a and b shows the Nyquist plots in the absence (blank) and presence of inhibitors **7b** or **8b** with the concentration ranging from 1 to 100 ppm. The inset figures (Fig. 6a and b) depict magnified form of Nyquist plots for blank and in the presence of 1 ppm inhibitor. The electrochemical equivalent circuit parameters were obtained by fitting the data using Nova (version 1.8) soft-ware. The electrochemical parameters of the fitted equivalent circuit were normalized using the specimen surface area (2 cm^2), are tabulated in Table 2. Bode plots for magnitude or phase angle *versus* frequency in Randle equivalent circuit are shown in Fig. 6c–f.

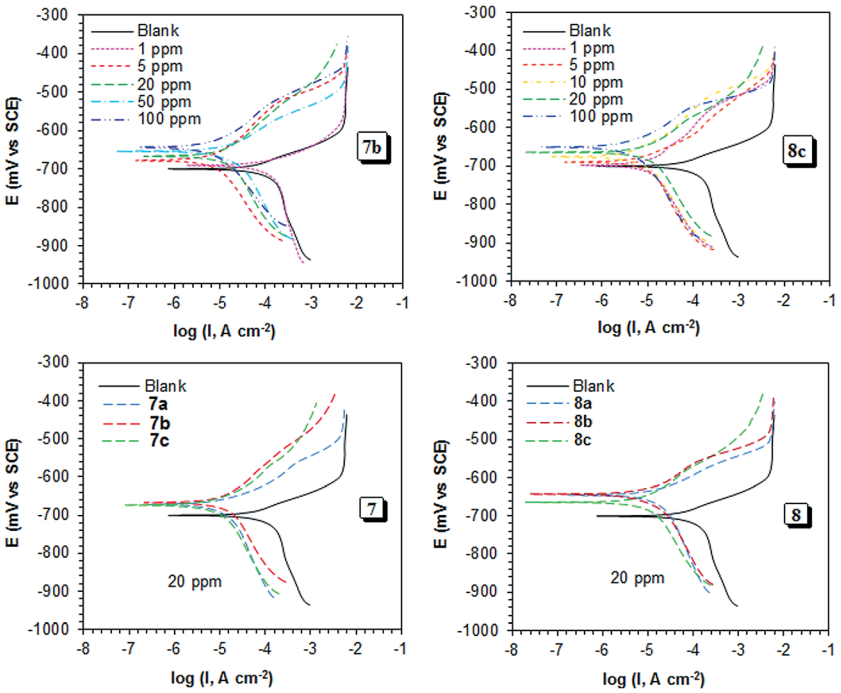

Fig. 4 Potentiodynamic polarization curves at 40 °C for mild steel in CO_2–saturated 0.5 M NaCl containing 1–100 ppm concentrations of (a) **7b** and (b) **8c**, and 20 ppm concentration of (c) **7** and (d) **8**.

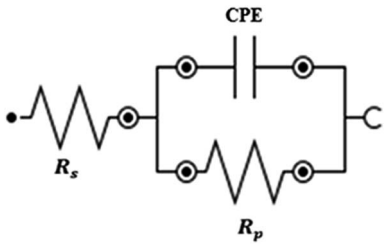

Fig. 5 Randles Electricalchemical equivalent circuit diagram used to modeling metal/solution interface. R_s: solution resistance, R_p: polarization resistance, CPE: constant phase element.

3.3. Adsorption isotherms

Fractional inhibition efficiency η and surface coverage θ are equal at lower concentration range of an inhibitor molecule, while their relationship does not remain linear at higher concentrations owing to a change of surface coverage from a monolayer to a multilayer coverage. The η values obtained by LPR method (Table 1) in CO_2–0.5 M NaCl and C were used to fit the following adsorption isotherms, namely:

$$\text{Temkin: } K_{ads}C = e^{f\theta} \quad (16)$$

$$\text{Langmuir: } \theta/(1-\theta) = K_{ads}C \quad (17)$$

$$\text{Frumkin:}^{38}\ K_{ads}C = \{\theta/(1-\theta)\}e^{-2\alpha\theta} \quad (18)$$

$$\text{Freundluich:}^{39}\ \theta = K_{ads}C^{n} \quad (19)$$

where K_{ads} is the equilibrium constant of the adsorption process. The data fitted the Langmuir isotherm the best as revealed by the correlation coefficient values (Fig. 7 and Table 3). Some of the inhibitors demonstrated a good fit for Temkin or Freundluich adsorption isotherms. The molecular interaction parameter f, which describes interactions of the inhibitor molecules in the adsorption layer as well as inhomogeneities on the electrode surface, was calculated from the Temkin isotherm (Table 3).[5,39] The K_{ads} is related to the free energy of adsorption (ΔG°_{ads}), by the eqn (20):

$$K_{ads} = \frac{1}{55.5}\exp\left(\frac{-\Delta G^{\circ}_{ads}}{RT}\right) \quad (20)$$

The values of K_{ads} and ΔG°_{ads} obtained from Langmuir isotherms are summarized in Table 3.

3.4. Gravimetric measurements in CO_2–0.5 M NaCl at 120 °C and a pressure of 10 bar

The results of the average of duplicate experiments carried out for 48 h using coupons of almost identical masses are given in Table 4. Eqn (21) was used to calculate percent inhibition efficiency (*i.e.* η%):

$$\eta\% = \frac{\text{weight loss (without inhibitor)} - \text{weight loss (inhibitor)}}{\text{weight loss (without inhibitor)}} \times 100 \quad (21)$$

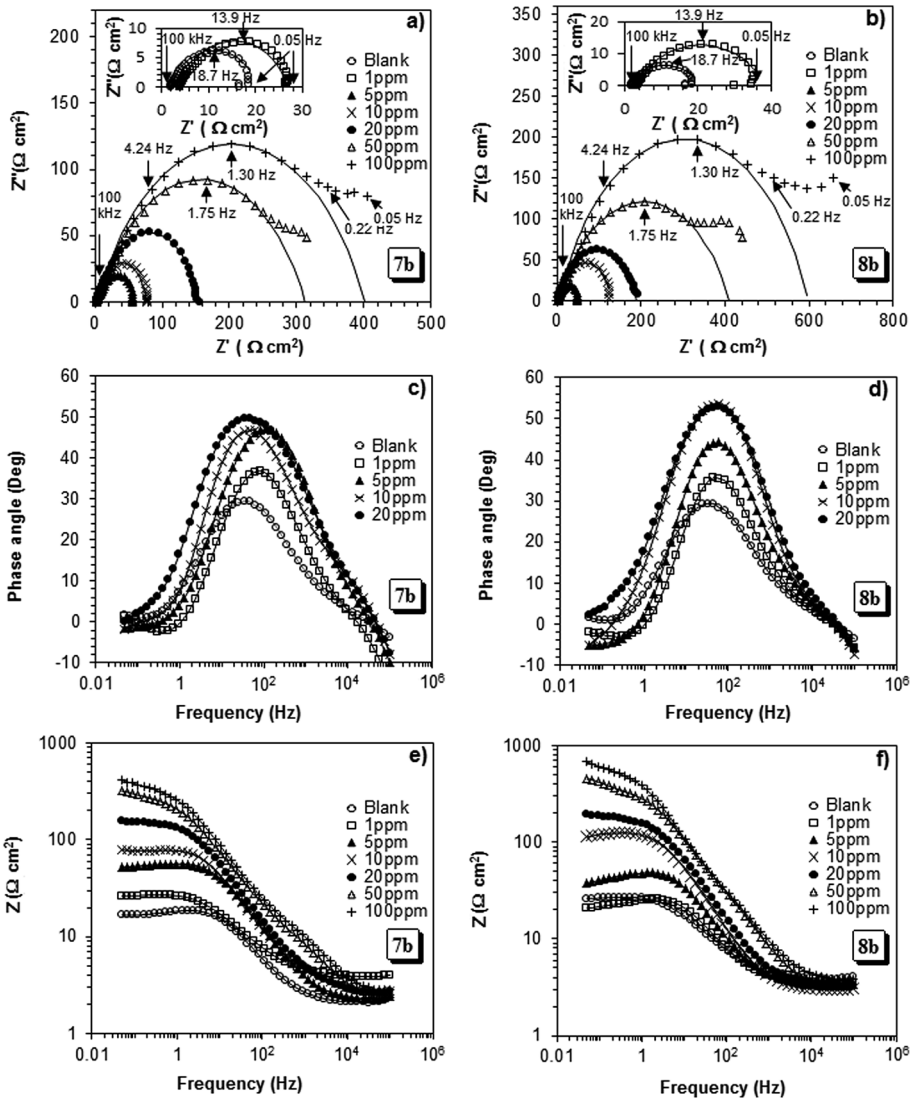

Fig. 6 Nyquist diagram of (a) **7b** and (b) **8b**, Bode phase angle plots of (c) **7b** and (d) **8b**, and impedance plots (e) **7b** and (f) **8b** of mild steel at 40 °C in CO_2 saturated 0.5 M NaCl containing various concentrations of inhibitors in 30 minutes immersion time. Solid line in the Nyquist plot fitted to the equivalent circuit; various symbols represent experimental data and solid lines represent fitted data.

In cases where the coupons differed in masses, relative weight loss of the coupons were used to determine the η%.[40,41] The average η% reported in the Table 4 is found to have a standard deviation of 2–3%.

3.5. Surface tension

The surface tension γ and CMC of IMs **7** and **8** are measured in 0.5 M NaCl, 0.5 M NaCl + CO_2 and water at 40 °C and the results are given in Table 5. Fig. 8a and b shows the plot of surface tension γ against the concentration of the IMs while Fig. 8c and d show the η% *versus* concentration profiles.

3.6. X-ray photoelectron spectroscopy

The intensity (counts) *versus* binding energy (eV) plots are displayed in Fig. 9. The XPS scan compositions of the metal surface are given in Table 6.

4. Discussion

A series of new IMs **7** and **8** having 4-mono-3,5-di- and 3,4,5-trioctyloxyphenyl substituents at C(2) and $(CH_2CH_2NH)_nH$ (n = 1 and 3) pendants at N(1) have been synthesized. The structural variation has permitted us to study the effects of hydrophobic electron-rich aromatic ring in shifting charge density to the coplanar N=C–N motifs as shown using **7a** (Scheme 2) as well as the effects of the number of hydrophilic amine groups in the pendants. A variety of nitrogen centers is expected to provide lone pair of electrons for the formation of coordinate-type bonds with the empty d-orbitals of Fe on the anodic sites of the metal surface. The presence of hydrophobic octyloxy chains is anticipated to provide ample surface coverage to safeguard the metal by entraining water layer from its surface into the hostile aqueous environment.

Table 2 Impedance parameters for the corrosion of a mild steel sample in various solutions containing inhibitors **7b** and **8b** in CO_2–0.5 M NaCl at 40 °C

Sample	Concentration (ppm by weight)	R_s (Ω cm^2)	R_p (Ω cm^2)	CPE[a] (μF cm^{-2})	n	R'_p (Ω cm^2)	η (%)
Blank		4.19	18.7	699	0.963	14.5	
7b	1	2.07	36.4	501	0.969	34.4	57.8
	5	2.3	59.1	227	0.963	56.8	74.5
	10	2.62	74.4	281	0.945	71.7	79.8
	20	3.1	152	307	0.926	149	90.3
	50	2.49	310	341	0.914	308	95.3
	100	2.89	400	306	0.791	397	96.3
8b	1	3.57	42.5	393	0.959	38.9	62.8
	5	3.4	47.2	301	0.906	43.8	66.9
	10	3.08	128	290	0.785	125	88.4
	20	3.47	186	268	0.653	183	92.1
	50	3.91	407	220	0.615	403	96.4
	100	5.88	591	226	0.599	585	97.5

[a] Double layer capacitance (C_{id}) and coating capacitance (C_c) are usually modelled with a constant phase element (CPE) in modeling an electrochemical phenomenon.

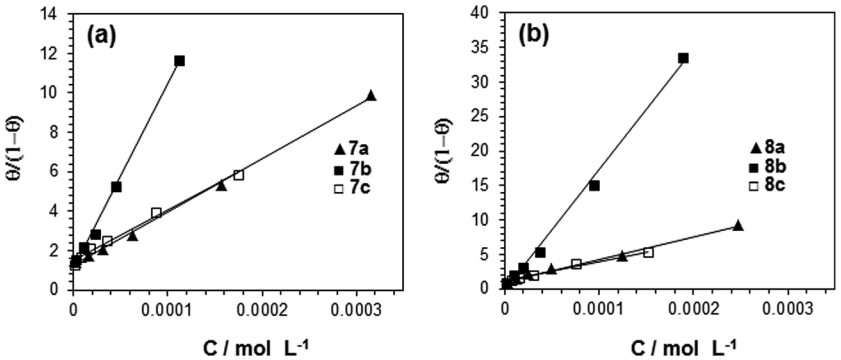

Fig. 7 Langmuir adsorption isotherm of (a) **7** and (b) **8** at 40 °C in CO_2 saturated 0.5 M NaCl solution.

The IMs in both series **7** and **8** demonstrated very good corrosion inhibition as determined by Tafel extrapolation and corroborated by LPR study (Table 1). In the presence of 100 ppm inhibitors, the LPR study revealed η% values 90.8, 96.7 and 85.4 for the DETA-derived IMs **7a**, **7b** and **7c**, respectively, while for the TEPA-derived inhibitors **8a**, **8b** and **8c**, the corresponding values were determined to be 90.2, 97.1 and 84.1 (Table 1). In all the concentrations studied, twin-tailed IMs **7b** and **8b** outperformed their mono- and triple-tailed counterparts **7a, c** and **8a, c**. It is quite possible that twin-tailed hydrophobe in 3,5-dispositions might actually be covering greater surface area of the metal than the triple-tailed IMs where hydrophobes in 3,4,5-dispositions may associate and occupy smaller space (bottom box, Scheme 2). In twin-tailed IMs, hydrophobe wings are spread out since the geometry in the 3,5-dispositions will not allow intramolecular association between them. It is a plausible

Table 3 Square of coefficient of correlation (R^2) and values of the constants in the adsorption isotherms of Temkin, Frumkin, Freundlich and Langmuir in the presence of inhibitors **7** and **8** in CO_2 saturated 0.5 M NaCl solution at 40 °C (LPR data from Table 2 used for the isotherms), and the equilibrium constant and free energy from the Langmuir isotherm

				Langmuir		
Compound	Temkin (R^2, f)	Frumkin (R^2, a)	Freundlich (R^2)	(R^2)	$K_{ads} \times 10^{-5}$ (L mol^{-1})	ΔG°_{ads} (kJ mol^{-1})
7a	0.9260, 14	0.7313, −3.5	0.9503	0.9984	27 083	−37.0
7b	0.9705, 12	0.7214, −2.7	0.9723	0.9973	93 424	−40.2
7c	0.9731, 15	0.9202, −4.9	0.9875	0.9868	25 723	−36.9
8a	0.9954, 10	0.9542, −2.4	0.9864	0.9919	32 676	−37.5
8b	0.9901, 9.2	0.7222, −1.1	0.9677	0.9949	175 082	−41.9
8c	0.9647, 13	0.9758, −0.78	0.9855	0.9866	28 555	−37.2

Table 4 Corrosion rates and inhibition efficiencies of corrosion inhibitors (200 ppm by weight) at 120 °C and 10 bar pressure of CO_2 in 0.5 M NaCl

Solution	Coupon[a]	CR[b] (mm y^{-1})	Inhibition efficiency (%)	Average inhibition efficiency (%)
Blank	A	2.19	—	—
	B	2.23	—	
7a	A	0.607	72.3	71.8
	B	0.638	71.4	
7b	A	0.45	79.7	80.6
	B	0.41	81.5	
7c	A	0.41	81.5	82.3
	B	0.38	83.1	
8a	A	0.569	74.0	72.5
	B	0.647	71.0	
8b	A	0.29	86.7	92.4
	B	0.23	89.6	
8c	A	0.26	88.1	93.3
	B	0.29	86.7	
Q I 80	A	0.429	80.4	81.0
	B	0.410	81.6	
ARMOHIB29	A	0.396	81.9	82.7
	B	0.368	83.5	

[a] Two mild steel coupons A and B having compositions. [b] Corrosion rate.

rationale supported by the experimental findings; however, at this stage, we do not have additional experimental evidence. Note that the variance in N(1) pendants did not impart any difference in their η%; pentamine derivatives **8** showed inhibition efficiencies similar to those of their triamine counterparts **7** (Table 1).

The results of the LPR method corroborated the findings of the Tafel extrapolations (Table 1). Some representative Tafel plots are shown in Fig. 4. As evident from the Table 1 and the Fig. 4, the IMs shifted the E_{corr} values towards less negative values (*i.e.* noble direction) with increasing inhibitor concentrations. In the presence of 100 ppm inhibitor, a shift in the range 35–73 mV does not qualify these inhibitors to be classified under the anodic type; a shift of at least 85 mV is suggested to be a requirement for an inhibitor to be classified as cathodic or anodic type.[42] It is evident from Fig. 4, the presence of the inhibitors causes slightly higher reduction in the current densities (i_{corr}) in the anodic than the cathodic branch. Inhibitor action is thus more pronounced in mitigating the iron dissolution at the anode than the cathodic reaction for hydrogen evolution. The IMs in the current work are thus considered as mixed-type inhibitors under the predominance of anodic control. At higher current densities, the slope of the cathodic branch is higher in absence of inhibitor. Within the limitation of an experimental error, the cathodic (β_c) and anodic slopes (β_a) are not changed considerably; the inhibitors simply block the anodic and cathodic reaction sites, and follow the same the mechanism of inhibition of the electrode reactions as discussed above. While negative ΔG°_{ads} values certify the favorability of the inhibitor adsorption process (Table 4);[43] the $-\Delta G^{\circ}_{ads}$ values in the range 37–41.9 kJ mol^{-1} is not large enough to described the adsorption mechanism by a chemisorption process. A value greater than 20 kJ mol^{-1} points towards involvement of both physi- and chemisorption of the IMs on the metal surface.[5,42] A protective film can be constructed by the formation of a coordinate type chemical bonds between d-orbitals of iron and the non-bonding as well as π-electrons in the electron-rich IM motif and the aromatic ring.[44]

Most of the anodic polarization curves in the current-*versus* potential plots exhibit desorption potentials as indicated by the presence of current-increasing before reached a plateau (Fig. 4).[44,45] The existence of desorption potential suggests a pathway in which the inhibitors initially block the anodic sites on the electrode and desorb at a higher potential leading to accelerated steel dissolution.

Electrochemical impedance spectroscopy (EIS) measurements were carried out to obtain better understanding of mild steel corrosion inhibition using various concentrations of **7b** and **8b** in CO_2–0.5 M NaCl at 40 °C (Fig. 6a and b). It has been found that increasing the concentrations of the inhibitors increases the diameter of the impedance semicircle. This can be attributed to increase in the adsorption of the inhibitors on the mild steel surface, thereby increasing the resistivity of the electrode. The figures show that the Nyquist diagrams do not adopt ideal semicircle where the capacitance at the inhibitor solution–metal interface does not exhibit a real capacitor. The depressed semicircle in the Nyquist plots obtained at high to medium frequency is characteristic to the solution–solid electrode interface that is associated with the surface roughness and inhomogeneity of the electrode.[46] The deviation from the semicircle shape in the Nyquist plots observed at low frequency for higher inhibitor concentration (50 and 100 ppm) solutions, indicate changing the electron transfer process including a diffusion-limiting step.[47]

As shown in Table 2, increasing the inhibitor concentration of **7b** continuously increases the value of R'_p, consequently the inhibition efficiency increase to its maximum value of 96.3% after 30 minutes of mild steel immersion in 100 ppm. Applying similar experimental conditions, the inhibition efficiency of **8b** was found to be 97.5%. Table 2 also shows that CPE value decreases with increasing the inhibitor concentration. This can be attributed to increase the roughness and inhomogeneity of the electrode surface because of increase the inhibitor

Table 5 Surface properties of IMs **7** and **8** in 0.5 M NaCl at 40 °C

Compound	Surface tension (mN m^{-1})	C_{cmc} (μmol L^{-1})	C_{cmc} (ppm)	ΔG°_{mic} (kJ mol^{-1})
7a	33.5	30.2	9.59	−27.1
7b	30.0	18.2	8.11	−28.4
7c	27.1	12.8	7.34	−29.3
8a	36.2	22.4	8.99	−27.9
8b	27.1	17.5	9.27	−28.5
8b[a]	32.0	23.4	12.4	−27.7
8b[b]	34.2	26.3	13.9	−27.4
8c	20.0	9.0	5.92	−30.2

[a] 0.5 M NaCl saturated with $C0_2$. [b] Salt-free water.

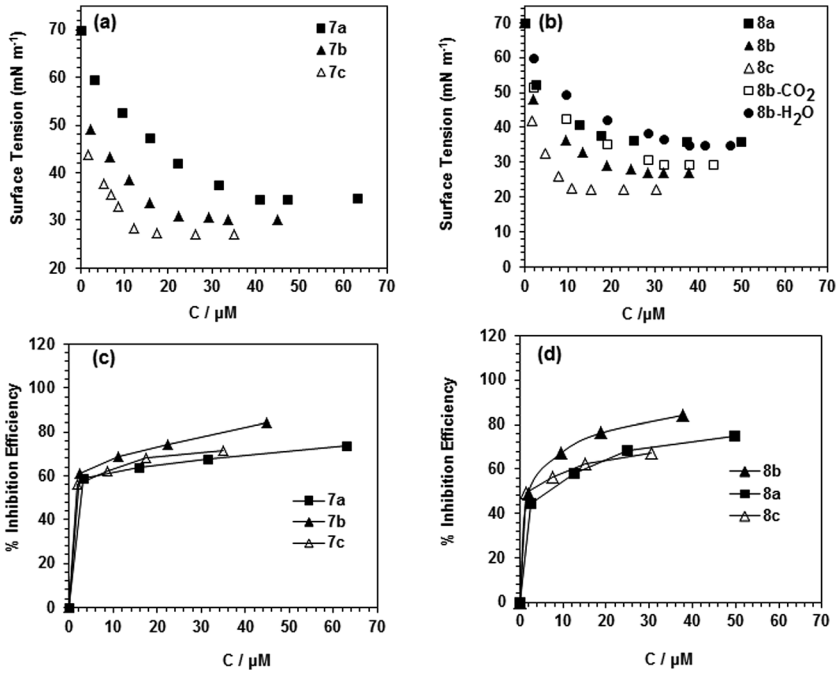

Fig. 8 Surface tension *versus* concentration of IM (a) **7** and (b) **8** in 0.5 M NaCl solution; and inhibition efficiency *versus* concentration of IMs (c) **7** and (d) **8** in CO_2 saturated 0.5 M NaCl solution at 40 °C.

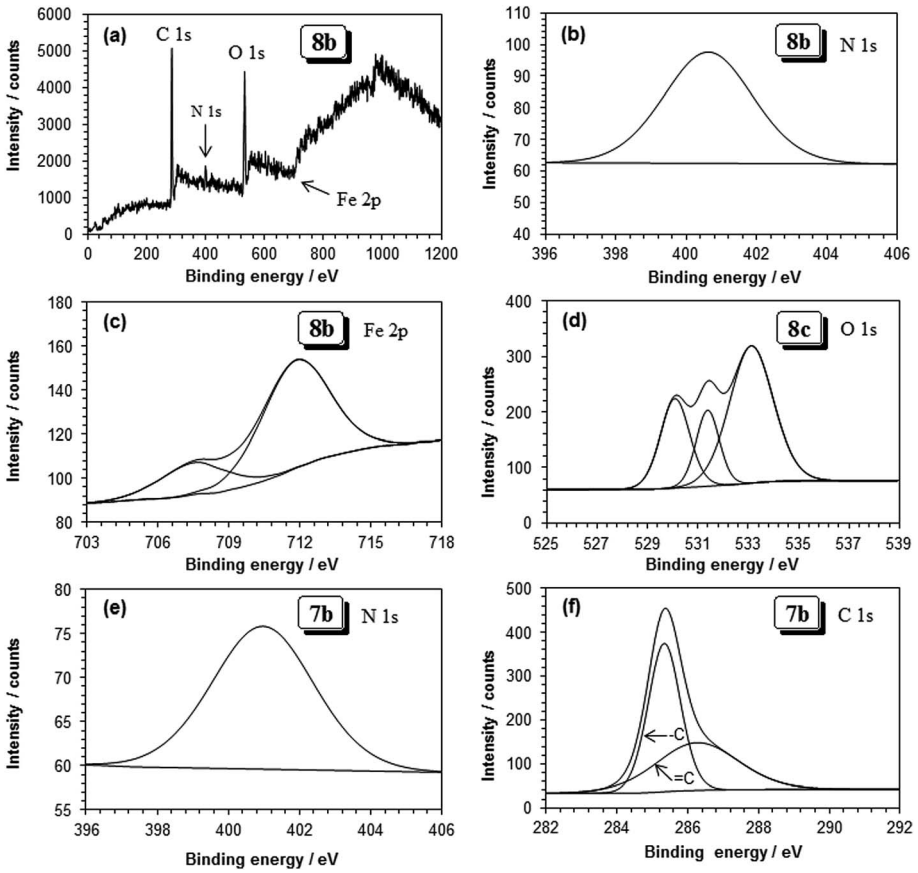

Fig. 9 (a) XPS survey spectrum and the XPS deconvoluted profiles of (b) N 1s, and (c) Fe 2p after immersing in CO_2 saturated 0.5 M NaCl at 40 °C for 6 h in the presence of **8b** (100 ppm); and (d) XPS deconvoluted profiles of O 1s in the presence of **8c** (100 ppm) and (e) N 1s and (f) C 1s in the presence of **7b** (100 ppm).

Table 6 XPS scan composition of Fe immersed in inhibited solution of 0.5 M NaCl–CO_2 (1 atom) at 40 °C for 4 h

Peak	Approx. binding energy (eV)	Composition (atom%)					
		7a	**7b**	**7c**	**8a**	**8b**	**8c**
C 1s	285.4	24.6	35.8	43.7	28.7	28.5	32.7
C 1s	286.5	37.8	29.4	19.9	22.8	38.0	32.2
O 1s	530.2	5.7	6.25	6.21	11.5	5.76	6.98
O 1s	531.3		1.52	0.71	14.4		4.72
O 1s	532.8	16.0	20.3	22.6	1.16		16.0
O 1s	533.7	9.54			11.4	20.1	
N 1s	400.2			3.33	4.94		5.15
N 1s	401.0	3.23	3.94			5.98	
Fe 2p	707.2		0.68	0.26		0.37	
Fe 2p	711.3	1.42	2.08	2.07	4.17	1.26	2.22
Fe 2p	714.2	0.78			0.81		
Cl 2p	197.6	0.9					
Cl 2p	198.8			1.24			

adsorption on the surface. The n values decrease with increasing concentrations of **7b** and **8b**. The lower n values at higher concentration of **7b** or **8b** can be attributed to increase the adsorption of the inhibitors on the surface of mild steel coupon, thereby suggested to increase the heterogeneity of their surface.

In Fig. 6c and d the value of R_s can be obtained from the horizontal plateau region at high frequency, it is almost constant and does not affect by increasing the inhibitor concentration in the solution.[48] However, at low frequency, the R_p can be determined from the Z magnitude, which increases with increasing the concentration of **7b** or **8b**; this is attributed to the increase in the polarization resistance value. Bode plot of phase angle *versus* frequency curve (Fig. 6e and f) shows a peak shape and maximum angle value at intermediate frequency increases with increasing the inhibitor concentration, which indicates the thickness of the surface increases as a result of additional amount of inhibitor adsorbed on the mild steel surface and consequently decrease the value of the capacitance. The results obtained from Nyquist and Bode plots confirmed the findings from the Tafel and LPR methods.

The surface coverage data (θ) indicate that the adsorption of the IMs are fitted best by the Langmuir adsorption isotherm; while some of them followed Temkin as well as Freundlich adsorption isotherms (Table 4). Note that higher values of f indicate energetic inhomogeneity of the metal surface.[49,50]

The inhibition efficacy η% in CO_2–0.5 M NaCl at 120 °C and pressure (10 bar) revealed that TEPA-derived IMs **8** performed better than their DETA-derived counterparts **7** in arresting corrosion as determined using two types of metal coupons A and B having different elemental compositions and carbon content. It is a great satisfaction to note that both twin- and triple-tailed IMs **8b** and **8c** performed much better than the two commercial IMs QI80 and ARMOHIB219 (Table 4).

The IMs having hydrophilic amidine motifs and hydrophobic alkyl chain pendants are considered as cationic surfactants because of the presence of cationic forms **II** and **IV** in equilibrium with **I** (Scheme 1).[51] In this work, CMCs of the IMs **7** and **8** have been determined in order to shed light on the adsorption process: do the IMs prefer micellization prior to adsorption or *vice versa*? As expected, the CMC as well as the surface tension at the CMC was found to be progressively lower as the number of alkyl tails increases.[34] Twin-tailed IM **8b** is determined to have CMC values of 26.3, 17.5 and 23.4 μM in salt-free water, 0.5 M NaCl, and CO_2/0.5 M NaCl, respectively (Table 5). The presence of NaCl makes the aqueous system more hostile environment for the hyhdrophobic tails which are thus encouraged to micellize resulting in a lower CMC value of 17.5 μM. In the presence of CO_2, formation of salts of types **II–IV** (Scheme 1) make the IM more water-soluble hence requiring higher concentration to reach the CMC value of 23.4 μM. For **8b** at a concentration of 10 ppm, the surface coverage (θ) of 76% confirms that the IM covers most of the surface before its concentration reach the CMC value of 12.4 ppm (*i.e.* 23.4 μM) in CO_2–saturated 0.5 M NaCl (Fig. 8, Table 5). The above data is validated by the finding that the adsorption on the metal surface is favored over the micellization as a result of ΔG°_{mic} (≈ -28 kJ mol^{-1}, Table 5) being lesser negative than ΔG°_{ads} (≈ -41 kJ mol^{-1}, Table 3). Individual inhibitor molecule is adsorbed on the metal surface to form a monolayer; after which adsorption of the micelles may impart further protection.[52]

The results of XPS survey of the surface of the metal coupons after immersion in 0.5 M NaCl–CO_2 containing inhibitors (100 ppm) are given in Table 6. The high carbon, small Fe, and the significant amount of N contents on the metal surface confirm the presence of a nitrogen- and carbon-aceous IM film (Fig. 9). As expected, the film of TEPA-derived IMs **8** contributed higher amount of N than their DETA-derived counterparts **7**. As an example, the XPS spectrum in the presence of inhibitor **8b** is shown in Fig. 9a. The XPS deconvoluted profiles of C 1s spectrum displayed a two-peak profile (*e.g.* Fig. 9f): the peak at 285.4 eV is assigned to the C–C aliphatic bonds, while the other peak suggests the presence of C=C, C=O, and C–N bonds. The O 1s spectra (*e.g.* Fig. 9d) revealed the presence of 2 to 4 peaks (Table 6): while the peaks at 530.2 and 531.3 eV are attributed to the O^{2-} in Fe_2O_3 and hydrous iron oxide FeOOH, peaks at 532.8 and 533.7 eV may account for the presence of the oxygen of adsorbed water.[20,53] The presence of Fe^{3+} (2p) and Fe^0 (2p) is revealed by the appearance of respective peaks at 711.3 and 707.2 eV, their small concentrations confirm the rather carbonaceous nature of the metal surface.

5. Conclusions

A new series of electron-rich IMs having hydrophobic electron-rich single-, twin-, and triple-tailed phenyl substituents at C(2) and hydrophilic *N*-pendants of $(CH_2CH_2NH)_nH$ (n = 1 and 3) have been synthesized. Twin-tailed IMs **7b** and **8b** imparted better inhibition of mild steel corrosion in CO_2–0.5 M NaCl at 40 °C than their single- and triple-tailed counterparts **7a**, **c** and **8a**, **c**, respectively. The changes in the *N*-pendants from CH_2-CH_2NH_2 in **7** to $(CH_2CH_2NH)_2CH_2CH_2NH_2$ in **8** seems to offer no advantage in corrosion at lower temperature and pressure, however at higher temperature (120 °C) and pressure (10 bar) **8b**

outperformed **7b** and two other commercial IM-based inhibitors. The greater reduction of i_{corr} values in the anodic branch of Tafel plots and the shift of the E_{corr} values in the anodic direction established that the IMs acted mainly as anodic inhibitors. The magnitude of ΔG°_{ads} values is indicative of chemisorption of the electron-rich amidine motifs by donation of electrons to the vacant d-orbitals in Fe on the anodic sites. The XPS results confirmed the formation of a protective IM film on the metal surface. The adsorption of the IMs was found to fit the Langmuir adsorption isotherm. The IMs are surface active molecules as they lower the surface tension; the surface coverage data and CMC values demonstrated that the inhibitor molecules prefers to undergo adsorption on to the metal surface rather than to micellize.

A better surface coverage provided by the twin-tailed IMs than their single- and triple-tailed counterparts is a significant finding that would indeed be helpful in designing better twin-tailed IMs having tails longer than the current octyloxy group.

Acknowledgements

Facilities provided by King Fahd University of Petroleum and Minerals and financial assistance by King Abdulaziz City of Science and Technology (KACST) (under the Grant: AR-26-26) are gratefully acknowledged.

References

1 M. Finšgar and J. Jackson, *Corros. Sci.*, 2014, **86**, 17–41.
2 W. Villamizar, M. Casales, J. G. Gonzalez-Rodriguez and L. Martinez, *J. Solid State Electrochem.*, 2007, **11**, 619–629.
3 A. H. Mustafa, B. Ari-Wahjoedi and M. C. Ismail, *J. Mater. Eng. Perform.*, 2013, **22**, 1748–1755.
4 M. B. Kermani and A. Morshed, *Corrosion*, 2003, **59**, 659–683.
5 W. Durnie, R. De Marco, A. Jefferson and B. Kinsella, *J. Electrochem. Soc.*, 1999, **146**, 1751–1756.
6 S. Ramachandran and V. Jovancicevic, *Corrosion*, 1999, **55**, 259–267.
7 K. Chokshi, W. Sun and S. Nesic, *Iron carbonate scale growth and the effect of inhibition in CO_2 corrosion of mild steel*, NACE International Corrosion Conference & Expo, Paper No. 05285, 2005.
8 D. M. Ortega-Toledo, J. G. Gonzalez-Rodriguez, M. Casales, L. Martinez and A. Martinez-Villafañe, *Corros. Sci.*, 2011, **53**, 3780–3787.
9 F. F. Eliyan and A. Alfantazi, *Corros. Sci.*, 2014, **85**, 380–393.
10 Q. Y. Liu, L. J. Mao and S. W. Zhou, *Corros. Sci.*, 2014, **84**, 165–171.
11 U. Lotz, L. Van Bodegom and C. Ouwehand, *Corrosion*, 1991, **47**, 635–644.
12 G. Zhang, C. Chen, M. Lu, C. Chai and Y. Wu, *Mater. Chem. Phys.*, 2007, **105**, 331–340.
13 S. Nesic and K. L. J. Lee, *Corrosion*, 2003, **59**, 616–627.
14 R. H. Hausler and D. W. Stegmann, *CO_2 Corrosion and its prevention by chemical Inhibition in oil and gas production*, Proceedings of Corrosion/88, NACE International, Houston, Taxes, paper no. 863, 1988.
15 S. Hernandez, J. Bruzual, F. Lopez-Linares and J. Luzon, *Isolation of potential corrosion inhibiting compounds in crude oils*, Proceedings of Corrosion/2003, NACE International, Houston, Taxes, paper no. 330, 2003.
16 X. Liu, S. Chen, H. Ma, G. Liu and L. Shen, *Appl. Surf. Sci.*, 2006, **253**, 814–820.
17 P. A. Koutentis, M. Koyioni and S. S. Michaelidou, *Molecules*, 2011, **16**, 8992–9002.
18 C.-H. Yu, C.-H. Huang and C.-S. Tan, *Aerosol Air Qual. Res.*, 2012, **12**, 745–769.
19 P. N. Sutar, A. Jha, P. D. Vaidya and E. Y. Kenig, *Chem. Eng. J.*, 2012, **207**, 718–724.
20 M. A. J. Mazumder, H. A. Al-Muallem and S. A. Ali, *Corros. Sci.*, 2015, **90**, 54–68.
21 W. Qiao, Z. Zheng and Q. Shi, *J. Surfactants Deterg.*, 2012, **15**, 533–539.
22 D. J. Heldebrant, P. G. Jessop, C. A. Thomas, C. A. Eckert and C. L. Liotta, *J. Org. Chem.*, 2005, **70**, 5335–5338.
23 V. Jovancicevic and S. Ramachandran, *Corrosion*, 1999, **55**, 631.
24 J. Cruz, L. M. R. Martınez-Aguilera, R. Salcedo and M. Castro, *Int. J. Quantum Chem.*, 2001, **85**, 546–556.
25 F. Farelas and A. Ramirez, *Int. J. Electrochem. Sci.*, 2010, **5**, 797–814.
26 P. C. Okafor, X. Liu and Y. G. Zheng, *Corros. Sci.*, 2009, **51**, 761–768.
27 B. Wang, M. Du, J. Zhang and C. J. Gao, *Corros. Sci.*, 2011, **53**, 353–361.
28 J. Zhang, G. Qiao, S. Hu, Y. Yan, Z. Ren and L. Yu, *Corros. Sci.*, 2011, **53**, 147–152.
29 M. Heydari and M. Javidi, *Corros. Sci.*, 2012, **61**, 148–155.
30 S.-H. Yoo, Y.-W. Kim, K. Chung, S.-Y. Baik and J.-S. Kim, *Corros. Sci.*, 2012, **59**, 42–54.
31 P. C. Okafor, C. B. Liu, Y. J. Zhu and Y. G. Zheng, *Ind. Eng. Chem. Res.*, 2011, **50**, 7273–7281.
32 M. W. S. Jawich, G. A. Oweimreen and S. A. Ali, *Corros. Sci.*, 2012, **65**, 104–112.
33 S. A. Ali, Y. Umar, B. F. Abu-Sharkh and H. A. Al-Muallem, *J. Polym. Sci., Part A: Polym. Chem.*, 2006, **44**, 5480–5494.
34 M. A. J. Mazumder, H. A. Al-Muallem, M. Faiz and S. A. Ali, *Corros. Sci.*, 2014, **87**, 187–198.
35 H.-J. Butt, K. Graf and M. Kappl, *Physics and Chemistry of Interfaces*, Wiley-VCH, Weinheim, 2003.
36 M. Erbil, *Chim. Acta Turc.*, 1988, **1**, 59–70.
37 M. Özcan, E. Karadag and I. Dehri, *Colloids Surf., A*, 2008, **316**, 55–61.
38 A. N. Frumkin, *Z. Phys. Chem.*, 1925, **116**, 466–484.
39 J. O. '. M. Bockris and S. U. M. Khan, *Surface Electrochemistry: A Molecular Level Approach*, Plenum press, New York and London, 1993.
40 S. A. Ali, M. T. Saeed and S. U. Rahman, *Corros. Sci.*, 2003, **45**, 253–266.
41 S. A. Ali, H. A. Al-Muallem, M. T. Saeed and S. U. Rahman, *Corros. Sci.*, 2008, **50**, 664–675.
42 S. Z. Duan and Y. L. Tao, *Interface Chemistry*, Higher Education Press, Beijing, 1990.

43 S. Nesic, G. T. Solvi and J. Enerhaug, *Corrosion*, 1995, **51**, 773–787.
44 F. Bentiss, M. Triasnel and M. Lagrenee, *Corros. Sci.*, 2000, **42**, 127–146.
45 W. Jia, *Chin. J. Oceanol. Limnol.*, 1998, **16**, 54–59.
46 R. Yildiz, T. Doğan and İ. Dehri, *Corros. Sci.*, 2014, **85**, 215–221.
47 X. Chen, Y. Wang, J. Zhou, W. Yan, X. Li and J.-J. Zhu, *Anal. Chem.*, 2008, **80**, 2133–2140.
48 I. L. Rozenfeld, *Corrosion Inhibitors*, MacGraw-Hill, New York, USA, 1981.
49 B. I. Podlovchenko and B. B. Damaskin, *Elektrokhimiya*, 1972, **8**, 297.
50 A. E. Stoyanova, E. I. Sokolova and S. N. Raicheva, *Corros. Sci.*, 1997, **39**, 1595–1604.
51 D. Bajpai and V. K. Tyagi, *J. Oleo Sci.*, 2006, **55**(7), 319–329.
52 K. Esumi and M. Ueno, *Structure performance relationships in surfactants*, Marcel Dekker Press, 2003.
53 M. Tourabi, K. Nohair, M. Traisnel, C. Jama and F. Bentiss, *Corros. Sci.*, 2013, **75**, 123–133.